TITLE: STABLE AND CLUMPED ISOTOPE SCLEROCHRONOLOGIES OF MUSSELS FROM THE BRAZOS RIVER, TEXAS (USA): ENVIRONMENTAL AND ECOLOGIC PROXY

AUTHORS: ALEXANDER A. VAN PLANTINGA[1], ETHAN L. GROSSMAN[1]

[1]Department of Geology and Geophysics, Texas A&M University, College Station, Texas, USA 77843-3115

ABSTRACT

Oxygen isotope sclerochronology with mollusk shells is complicated in subtropical regulated rivers by irregular shell $\delta^{18}O$ patterns. We performed multi-proxy analyses ($\delta^{18}O$, $\delta^{13}C$, clumped isotopes) from serially-sampled freshwater mussels in two species (*Amblema plicata* and *Cyrtonaias tampicoensis*), two specimens each, from the Brazos River, Texas to age specimens and test whether they accurately record environmental conditions such as river discharge and water source. Oxygen isotopic measurements are similar to predicted aragonite $\delta^{18}O$ values based on temperature and water $\delta^{18}O$, but the record is complex and irregular. To better resolve the chronologies, we performed clumped isotope analyses on select shell intervals. Clumped isotope temperatures ($T(\Delta_{47})$) ranged from 19° to 36°C. Summer $T(\Delta_{47})$ values were 3-5°C higher than measured temperatures, suggesting an offset in paleothermometer calibration. Chronologies based on Δ_{47} and $\delta^{18}O$ reveal specimen ages of 3-4 years and winter growth cessation or dramatic slowing in both *C. tampicoensis* and *A. plicata*, highlighting thermal limitations on growth and potential biases in environmental reconstructions. Carbon isotope trends were similar between conspecific shells, but differed between species, with mean $\delta^{13}C$ of -9‰ for *A. plicata* and -12‰ for *C. tampicoensis*. These findings argue for more direct environmental control on the *A. plicata* shell $\delta^{13}C$ chronology, which correlates with upstream dam releases. Furthermore, a relationship between river discharge and water $\delta^{18}O$ can be used to reconstruct the timing of high discharge based on shell $\delta^{18}O$.

KEY WORDS: mussels, stable isotopes, clumped isotopes, rivers, sclerochronology

1. INTRODUCTION

Sclerochronology is the science of reconstructing environmental and growth history from invertebrate hard parts such as mollusk shells or corals. Freshwater mussel (Unionidae) shells hold promise as environmental recorders, depositing layers of shell calcium carbonate that can reflect environmental conditions such as temperature, water $\delta^{18}O$ and dissolved inorganic carbon (DIC) $\delta^{13}C$, food availability, salinity, and river discharge (Dettman et al., 2004; Carroll et al., 2006; Goewert et al., 2007; Versteegh et al., 2010a; Versteegh et al., 2010b; Kelemen et al., 2017). Furthermore, $\delta^{18}O$ in shell growth layers is widely used to reconstruct shell growth chronology, permitting aging of specimens. Shell $\delta^{13}C$ can also chronicle environmental conditions, but metabolic effects can complicate interpretation. Aquatic mollusk shell carbon comes from DIC that may reflect watershed lithology, air-water exchange, and respired CO_2, further modified by metabolic effects on carbonate ions incorporated into the shell during biomineralization (McConnaughey and Gillikin, 2008).

The oxygen isotopic compositions of mollusk shells depend on the $\delta^{18}O$ of the ambient water ($\delta^{18}O_{WATER}$) and the temperature of mineralization (~-1‰ per 5˚C; Epstein et al., 1953; Grossman and Ku, 1986). Thus, paleoclimate interpretations of carbonate $\delta^{18}O$ often hinge on constraining the effects of temperature or water $\delta^{18}O$ (e.g., Ivany et al., 2004), such as studying marine environments where $\delta^{18}O_{WATER}$ varies minimally (e.g., Schöne et al., 2003). In contrast, isotopic studies of freshwater environments such as rivers are hampered by variability in $\delta^{18}O_{WATER}$ and temperature. Nevertheless, oxygen isotope studies of mussels from unregulated temperate rivers, subject to large temperature variations, can effectively distinguish seasonal cycles of growth (Dettman et al., 1999; Versteegh et al., 2010a).

Application of multiply substituted isotopologues, or "clumped isotopes" to estimate shell growth temperature can resolve the ambiguity between water $\delta^{18}O$ and temperature. Clumped isotope techniques have recently been introduced to resolve ambiguous shell $\delta^{18}O$ values in marine bivalves (Keating-Bitonti et al., 2011). This technique has not yet been used to measure spatially fine (< 1 mm thick) and thus temporally fine (< 60 days) shell growth layers in freshwater mussels (Unionidae). Doing so can facilitate calibration of shell $\delta^{18}O$ and temperature to river $\delta^{18}O$ and temperature, particularly with shell records that are difficult to interpret, in order to develop a shell proxy record of environmental conditions.

Besides providing environmental information, isotopic studies of unionids can provide vital ecologic information on taxa that are regarded as imperiled worldwide (Lydeard et al. 2004). Freshwater mussel populations are especially threatened by dams that alter river discharge, sediment loads, and water temperature regimes (Richter et al. 1997). Dams account for the 195 major reservoirs (> 5,000 acre-ft) in the state of Texas (Ward, 2012). Such damming alters mussel species composition by fragmenting habitats for mussels and host fish (Randklev et al., 2013). Freshwater mussel populations in the watershed of the Brazos River, the largest river in Texas, have been shown to decline with increasing proximity to dams (Randklev et al., 2013; Tsakiris and Randklev, 2016). Investigations into the chemical and isotopic chronologies archived in unionid shells can help to better characterize mussel growth patterns, metabolic activity, reproductive investment, and responses to environmental variables such as river discharge, water source, and temperature.

The negative impact that dams have on mussels and their host fishes is accompanied by ecosystem-wide disturbances (Freeman et al., 2003). Ecological variation could account for some of the ontological variation that malacologists observe in North America (Haag, 2012). It is

poorly understood how dams can dampen or amplify seasonal cycles for tracers like salinity, temperature, $\delta^{18}O$, and $\delta^{13}C_{DIC}$, but comparing modern shell chemistry with shells that grew prior to dam construction can help model dam impacts on environments.

In this study we used high-resolution stable isotope analyses along with clumped isotopes to reconstruct shell growth chronologies in two common species of freshwater mussel, Tampico Pearlymussel (*Cyrtonaias tampicoensis*) and Threeridge (*Amblema plicata*), collected from the Brazos River near College Station, Texas. Using common species makes this study easier to reproduce in other drainage basins. Sclerochronologies were developed based on $\delta^{18}O$ values predicted from coeval isotope and temperature data for Brazos River water. Clumped isotope measurements served as a secondary criterion in developing the sclerochronologies. The chronologies were then evaluated for their use in reconstructing river discharge, salinity (measured as electrical conductivity, or EC), and water source. Lastly, one specimen each of Threeridge and Tampico Pearlymussel, historically collected (1880-1920) from the study area prior to major dam construction in the Brazos watershed, were evaluated using the same techniques to explore isotope signals and thus environmental conditions before and after dam construction on the Brazos River.

2. STUDY AREA AND METHODS

2.1. Study Area and Samples

89 The study site on the Brazos River near College Station, Texas is about 210 km north of
90 Freeport, Texas, where the Brazos flows into the Gulf of Mexico (Figure 1). This study focuses
91 on the middle Brazos run, flowing southeast through a semi-arid to semi-humid climate
92 characterized by hot summers and mild winters, averaging 29˚C and 13˚C, respectively (Nielsen-
93 Gammon, 2012). Average annual rainfall is 100 cm and historically peaks in late-spring and mid-
94 fall. About 240 km upstream of the study site is Lake Whitney, dammed for hydropower and
95 flood control. About 30 km upstream of the study site is the confluence with the Little River, the
96 largest Brazos tributary, receiving output from Lake Belton, Stillhouse Hollow Lake, and
97 Granger Lake, all dammed reservoirs. From January 2012 through July 2013, weekly
98 temperature measurements and water $\delta^{18}O$ samples were collected from the Brazos River at the
99 Highway 60 bridge between Brazos and Burleson counties (Van Plantinga et al., 2016).

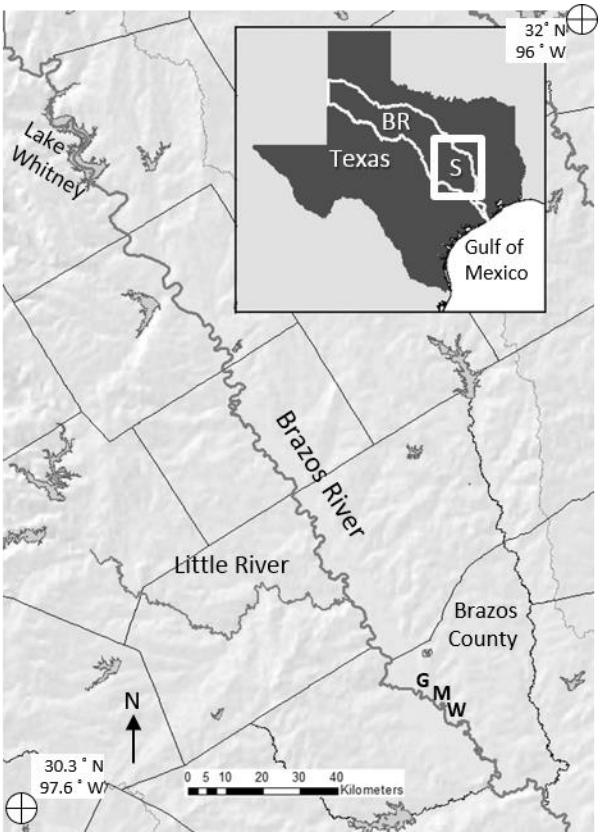

Figure 1. Study area. Inset: Map of Texas, Brazos River watershed (BR), and study area (S). The map reaches from Lake Whitney in the north to Brazos County in the south, where the water collection (W), mussel collection (M), and gage (G, USGS gage 08108700) locations are.

Modern specimens of *Amblema plicata* and *Cyrtonaias tampicoensis* were collected live on August 9, 2013 from the Brazos River near the Highway 60 bridge, from a muddy to sandy bank margin habitat at depths shallower than 2 m. Two historical specimens, one *A. plicata* (H3R) and one *C. tampicoensis* (HTP), both mature adults, were loaned from the Singley Collection from the University of Texas at Austin Non-Vertebrate Paleontology Lab. These specimens were collected sometime between 1880 and 1920 in the Brazos River near Bryan-College Station.

We performed isotope analyses on two young adult specimens each of modern *A. plicata* (labelled 3R3 and 3R5) and *C. tampicoensis* (TP2 and TP3), and on the two historical specimens (H3R and HTP). Specimen lengths varied from 70 mm (3R5) to 99 mm (HTP; Table 1). Specimens were sectioned with an Isomet saw from hinge to ventral margin perpendicular to growth bands. The shell sections were then manually broken in two to mount and epoxy on glass slides (Figures 2A and 2B). Mussel ages were initially estimated by counting growth bands, a common but imperfect method because of the deposition of non-periodic bands due to sudden stress (Neves and Moyer, 1988). Estimated mussel ages upon death ranged from 3-7 years old for the four modern specimens and 7-12 years old for the historical specimens (Table 1). Ages were also estimated using shell length and the von Bertalanffy equation (Haag and Rypel, 2011):

$$L_t = L_{inf}(1 - e^{-K(t-t_o)}) \quad (1)$$

where L_t is length in mm at shell age t in years, L_{inf} is length after infinite years, K is the growth constant, and t_0 is the time when shell length is 0 mm. Using *A. plicata* growth constants of 0.074 and 0.207 y^{-1} from Haag and Rypel (2011) and Christian et al. (2000) yields ages ranging from 5

to 14 years for our *A. plicata* shells, and growth rates for the outer 1 mm of 2-9 mm/yr (0.17-0.75 mm/month). Our stable isotope chronologies below will test these shell age estimates.

Table 1. Sample length, ages estimated by isotope sclerochronology (in modern shells) and by band counting(in historical shells), and growth rates for specimens of modern (M) and historic (H) Threeridge (*Amblema plicata*) and Tampico pearlymussel (*Cyrtonaias tampicoensis*). Because historical shells were aged by growth band counts, the minimum estimated age is one less than the minimum number of countable growth bands in order to account for the tendency to overestimate age by this method. K values were calculated assuming L_{inf} of 110 mm for Threeridge (Haag and Rypel, 2011) and L_{inf} 160 mm for Tampico pearlymussel (Howells, 2014).

Specimen	Age	Length (mm)	Growth bands	Estimated age min (y)	K (y^{-1})	Estimated age max (y)	K (y^{-1})
Threeridge							
3R5	M	70	2-7	3	0.346	4	0.259
3R3	M	71	3-7	3	0.337	4	0.253
H3R	H	91	9-10	8	0.220	10	0.176
Tampico pearlymussel							
TP2	M	95	2-7	3	0.300	4	0.225
TP3	M	97	3-7	3	0.311	4	0.233
HTP	H	99	6-9	5	0.193	9	0.107

2.2. Stable Isotope Measurements and Predicted $\delta^{18}O$ Values

Water samples were measured for $\delta^{18}O$ and δD using a Picarro L2120i cavity ringdown spectrometer at the Stable Isotope Geoscience Facility at Texas A&M University (TAMU). Calibrations are described in Van Plantinga et al. (2016). Brazos River discharge data from the gage at Highway 21 near College Station (USGS 08108700) were obtained online from http://waterdata.usgs.gov/tx. Sample powders were collected from shell cross-sections along growth layers with a New Wave micromill using a 0.5 mm drill bit following the methods of Dettman and Lohmann (1995). In each shell, two transects were milled, one across the ventral margin area (also referred to as the outer nacreous layer or ONL), and one across the inner nacreous layer area (INL) near the hinge of the shell (Figure 2). In specimen HTP, we analyzed duplicates of powder drilled from a cross section of the ventral margin. All sample intervals were

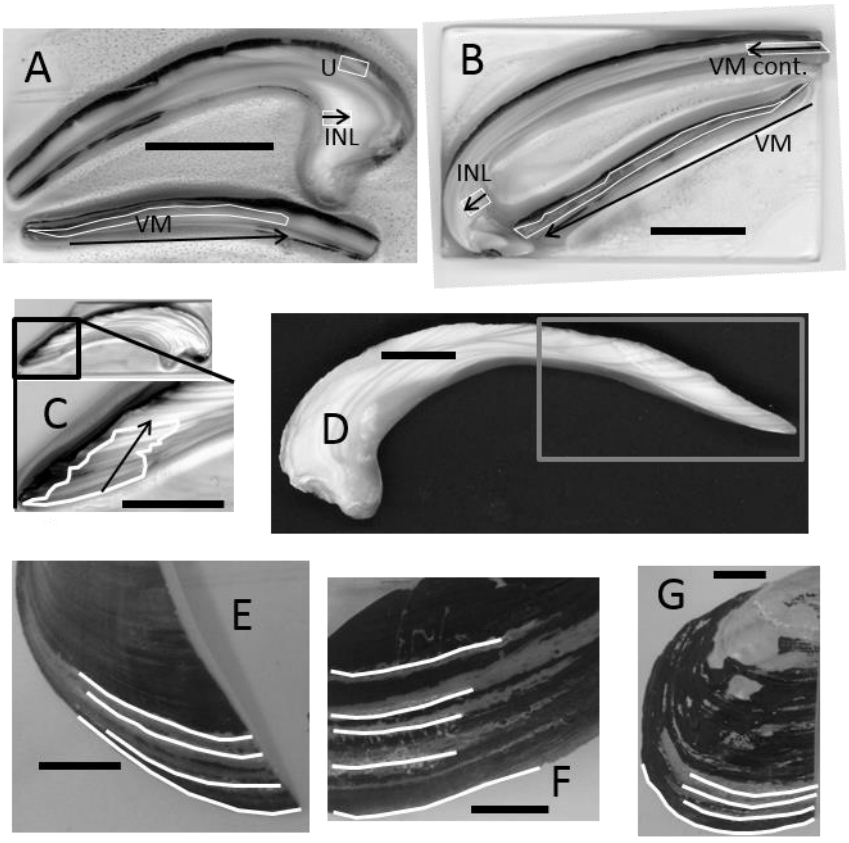

Figure 2. Images of sectioned specimens 3R5 (A) and TP2 (B). Micro-sampling transects are outlined in white with arrows indicating direction of sampling. VM is ventral margin, INL is inner nacreous layer, and U is umbo. Figures 2C and 2D show the sampling regions for H3R and HTP, respectively. Figures 2E, 2F, and 2G depict the clumped isotope sample regions, outlined in white, in specimens 3R5, TP2, and H3R, respectively. Scale bars are 1 cm.

between 60 and 140 µm, with generally shorter spacing for INL than ONL. Stable isotope results are plotted by shell thickness as in Dettman et al. (1999), rather than distance from umbo as in Versteegh et al. (2010a). The modern *A. plicata* specimens were also sampled for stable isotopes along the umbos of the shells to compare ontogenetically early and late carbon isotope values. For isotopic analyses, ~60 µg of powder were reacted with phosphoric acid (ρ = 1.92 mg/ml) in a Kiel IV carbonate reaction system at 75 °C and the CO_2 analyzed on a Thermo Finnigan MAT 253 mass spectrometer at the Stable Isotope Geosciences Facility at Texas A&M University (TAMU). Average analytical precision was 0.05‰ for $\delta^{18}O$ and 0.03‰ for $\delta^{13}C$ based on replicates of the NBS-19 internal lab standard used in every set of analyses.

Temperature and water $\delta^{18}O$ data, along with the aragonite oxygen isotope thermometry equation from Dettman et al. (1999; based on Grossman and Ku, 1986), were used to predict shell $\delta^{18}O$ values based on temperature (T) in Kelvin and $\delta^{18}O$ water in VSMOW ($\delta^{18}O_{WATER}$), as follows:

$$1000 \ln (\alpha_{water}^{aragonite}) = 2.559 (10^6 T^{-2}) + 0.715 \quad (2)$$

$$\alpha_{water}^{aragonite} = \frac{\left(1000+\delta^{18}O_{aragonite_{VPDB}}\right)}{\left(1000+\delta^{18}O_{water_{VSMOW}}\right)} \quad (3)$$

$$\alpha_{VPDB}^{VSMOW} = 1.0309 \text{ (Gonfiantini et al., 1995).} \quad (4)$$

2.4. Clumped Isotope Measurements of Shells

In order to assign temperatures to shell growth intervals and determine the differences, if any, between light and dark growth layers, clumped isotope samples were taken from distinct light and dark bands within the micromilled ventral margin transects in specimens 3R5 and TP2.

Select light and dark bands in historical shells H3R and HTP were sampled for clumped isotope measurements. After removing the periostracum with sandpaper, samples were taken from the top of the shell parallel to growth bands using a Dremel drill with a 0.5 mm dental bur on a low speed setting (Figures 2E, F, and G). Sample powders were analyzed for $\delta^{13}C$, $\delta^{18}O$ and Δ_{47} at Johns Hopkins University (JHU) during March 2015 on a Thermo Scientific MAT 253 mass spectrometer. Carbonate powders were converted to CO_2 gas using a custom automated acid-digestion and sample purification line with a common acid bath of phosphoric acid (ρ = 1.91 mg/ml) at 90 ˚C (see Henkes et al., 2013, for details). Three to four replicate analyses of ~8 mg each were performed per growth layer sampled.

Internal clumped isotope standards and reference gases from January 21-April 12 2015 were used for quality assurance and reference frame purposes. Daily isotope measurements of CO_2 gases equilibrated at 30 ˚C and 1000 ˚C were performed to make a Δ_{47} transfer function in an absolute reference frame known as the carbon dioxide equilibrium scale (Dennis et al., 2011). Raw $\delta^{18}O$ and $\delta^{13}C$ data were calibrated to the VPDB scale using NBS-19. Two internal standards were used daily to monitor performance: 102-GC-AZ01 (n = 33) with Δ_{47}, $\delta^{18}O$, and $\delta^{13}C$ of 0.697 ± 0.029‰, -14.46 ± 0.09‰, and 0.45 ± 0.06‰, respectively; and HAF-Carrara (n = 19) with Δ_{47}, $\delta^{18}O$, and $\delta^{13}C$ of 0.398 ± 0.010‰, -1.80 ± 0.03‰ and 2.29 ± 0.01‰, respectively. The standards 102-GC-AZ01, HAF-Carrara, and NBS-19, measured in triplicate, had Δ_{47} standard deviations 0.014, 0.006, and 0.008 per mil, respectively, averaging to ± 0.009 per mil, which equates to ± 4 ˚C paleotemperature error at the collective shell sample Δ_{47} average of 0.674 per mil using Henkes et al. (2013). For paleotemperatures we used the equation for mollusk and brachiopod shells presented in Henkes et al. (2013):

$$\Delta_{47} = 0.0327 * 10^6 / T^2 + 0.3286 \quad (4)$$

3. RESULTS

Measured $\delta^{18}O$ and $\delta^{13}C$ values of the ventral margin (VM), inner nacreous layer (INL), and umbo (U) in each shell are summarized in Table 2. Similar $\delta^{18}O$ trends and values are seen in all four VM records (Figure 3), with three of the four records showing a decreasing trend of minima (peaks in Fig. 3) of less than -3‰. The only exceptions are the values as low as -4.6‰ at ~1.6 mm in specimen 3R5. The $\delta^{18}O$ values and trends in paired VM-INL transects are nearly identical, except that INL records are of lower resolution because of either the lower growth rate relative to the ventral margin or increased rates if dissolution and reprecipitation in the INL. Four distinctive $\delta^{18}O$ minima can be used as correlation points (W, X, Y, Z). All are < -3‰ and at least 1‰ lower than the adjacent maxima.

Whether comparing different shells or paired VM-INL transects, the $\delta^{13}C$ values and trends in Threeridge mussels are similar, with $\delta^{18}O$ minima "X" correlating with the most distinctive $\delta^{13}C$ maxima (troughs in Figures 3). Curiously, the average $\delta^{13}C$ values of the ontogenetically younger portion of the umbo area (-7 to -6‰) is significantly greater than those of the older ventral margin regions of the shells (-10 to -9‰). The $\delta^{13}C$ records for Tampico pearlymussel differ between shells and between VM and INL transects within shells. Moreover, the modern Tampico shell $\delta^{13}C$ is 2.6‰ lower on average than the Threeridge shells (-12.0 ± 0.5‰ versus -9.4 ± 0.3‰).

Table 2. Summary of shell carbon and oxygen isotopic compositions for ventral margin (VM), inner nacreous layer (INL), and umbo (U) regions for modern (M) and historic (H) Threeridge (*Amblema plicata*) and Tampico pearlymussel (*Cyrtonaias tampicoensis*). G is growth rate in mm/yr.

			$\delta^{18}O$ ‰				$\delta^{13}C$ ‰				
Specimen	Age	Region	x̄	σ	min	max	x̄	σ	min	max	N
Threeridge											
3R5	M	VM	-2.8	0.8	-4.6	-1.3	-9.3	1.7	-14.2	-6.7	58
		INL	-2.7	0.8	-4.7	-1.5	-9.1	1.9	-13.3	-6.0	48
		U	-3.2	0.8			-6.8	1.9			
3R3	M	VM	-2.8	0.7	-4.6	-1.4	-9.8	1.4	-13.2	-7.0	57
		INL	-3.1	0.2	-5.0	-1.3	-9.2	1.6	-12.4	-6.7	32
		U	-2.6	1.1			-6.0	1.6			
H3R	H	VM	-3.8	0.8	-5.3	-1.8	-9.5	0.6	-10.6	-7.9	56
Tampico Pearlymussel											
TP2	M	VM	-2.8	1.0	-4.5	-0.4	-12.2	2.1	-16.6	-8.9	43
		INL	-3.2	0.6	-4.1	-2.0	-11.3	1.7	-14.6	-8.7	25
TP3	M	VM	-2.7	0.6	-4.4	-1.3	-12.4	2.0	-16.8	-8.9	62
		INL	-2.8	0.8	-4.5	-1.1	-12.1	2.2	-14.9	-7.9	34
HTP	H	VM	-3.2				-11.6				2

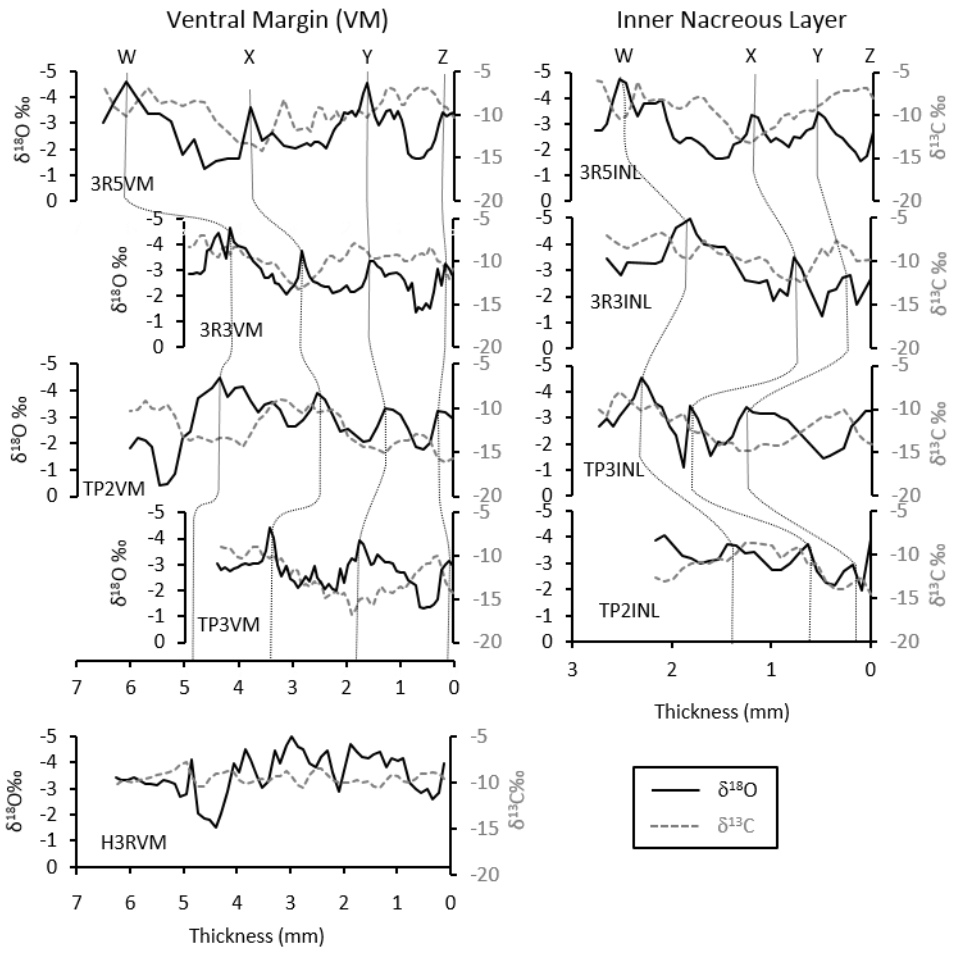

Figure 3. Oxygen (black line) and carbon (gray dashed line) isotope data for ventral margin (VM, left) and inner nacreous layer (INL, right) intervals from the four modern shells with correlation tie points W, X, Y, Z. Ventral margin data for the historical Threeridge specimen H3R is shown at bottom left.

Clumped isotope temperatures and $\delta^{18}O_{WATER}$ calculated from clumped temperatures ($\delta^{18}O_{WATER\_\Delta47}$) using shell $\delta^{18}O$ values and the ^{18}O paleotemperature equation of Dettman et al. (1999), are presented in Table 3. The 3R5 measurements yield two cool temperatures (21 ± 3 ˚C and 19 ± 3 ˚C) and two warm temperatures (32 ± 4 ˚C, 33 ± 3 ˚C). The TP2 clumped isotope temperatures vary from 26 ± 5 ˚C to 36 ± 2 ˚C. The clumped temperatures at the shell ventral margins are higher than the measured water temperatures within the 30 days preceding the shell collection date by 3 ˚C in 3R5 and 5 ˚C in TP2. This discrepancy between measured and

234 clumped temperatures may indicate a problem with either the environmental measurements or

235 the clumped temperature calibration, as discussed later.

Table 3. Sample $\delta^{18}O$, $\delta^{13}C$, Δ_{47}, clumped isotope temperature, and calculated $\delta^{18}O_{water}$ with associated precisions. Temperatures were calculated using the paleotemperature equation from Henkes et al. (2013). The column "B" stands for banding, "D" is dark, and "L" is light. Entries for "all" summarize mean and standard deviation of clumped isotope temperature and $\delta^{18}O_{WATER\_\Delta47}$ calculations for each shell.

Sample	Shell thickness interval (mm)	N	$\delta^{18}O$ (‰)	σ	$\delta^{13}C$ (‰)	σ	Δ_{47} (‰)	σ	T (°C)	σ	$\delta^{18}O_{WATER\_\Delta47}$ (‰)	σ	B
3R5	0.3	4	-2.62	0.05	-10.13	0.02	0.667	0.006	33	3	-1.3	0.5	D
	0.9	3	-2.60	0.10	-8.63	0.15	0.668	0.009	32	4	-1.4	0.7	D
	3.9	3	-1.70	0.14	-10.80	0.10	0.697	0.008	21	3	-2.7	0.5	L
	4.6	4	-1.20	0.05	-10.69	0.05	0.700	0.007	19	3	-2.5	0.5	D
	all	14	-2.03	0.70	-10.06	1.00	0.683	0.018	26	7	-2.0	0.7	
TP2	0.3	4	-2.46	0.11	-12.64	0.03	0.661	0.012	35	5	-0.7	0.9	L
	1.4	4	-2.17	0.04	-10.98	0.24	0.684	0.012	26	5	-2.3	0.9	L
	2.7	3	-3.13	0.06	-9.29	0.14	0.671	0.001	31	1	-2.2	0.1	L
	3.2	3	-2.83	0.15	-8.62	0.02	0.661	0.005	36	2	-1.1	0.5	L
	4.9	3	-2.71	0.04	-12.95	0.01	0.678	0.010	28	4	-2.3	0.8	D
	all	17	-2.66	0.36	-10.90	1.94	0.671	0.010	31	4	-1.7	0.8	
H3R	0.3	4	-5.07	0.04	-11.25	0.02	0.659	0.009	36	4	-3.2	0.7	D
	2.0	3	-4.17	0.00	-9.86	0.02	0.681	0.004	27	2	-4.0	0.4	D
	4.3	3	-2.47	0.13	-9.94	0.03	0.672	0.007	31	3	-1.6	0.4	L
	5.7	3	-3.27	0.03	-10.41	0.02	0.671	0.009	31	4	-2.3	0.9	D
	40	3	-3.70	0.08	-8.36	0.02	0.680	0.014	27	6	-3.4	1.2	D
	all	16	-3.74	0.97	-9.96	1.05	0.673	0.009	30	4	-2.9	0.9	
HTP	0.3	3	-4.04	0.03	-9.69	0.02	0.683	0.002	26	1	-4.0	0.1	L
	1.0	3	-2.44	0.07	-10.46	0.00	0.677	0.004	29	2	-2.0	0.3	D
	3.0	4	-2.52	0.02	-12.83	0.04	0.663	0.008	35	4	-0.9	0.7	L
	6.0	3	-3.82	0.03	-10.36	0.03	0.673	0.009	30	4	-3.1	0.7	D
	25	3	-3.62	0.10	-11.97	0.03	0.674	0.010	30	4	-2.9	0.7	D
	all	16	-3.29	0.75	-11.06	1.29	0.674	0.007	30	3	-2.6	1.2	

236 Oxygen and clumped isotope results were compared between modern (3R5 and TP2) and

237 historical specimens (H3R and HTP) by t-test. Only shell $\delta^{18}O$ and $\delta^{18}O_{WATER\_\Delta47}$ significantly

238 differed ($p < 0.05$) between modern and historical shells. Average $\delta^{18}O$ is -2.3‰ in modern

239 shells and -3.5‰ in historical shells. $\delta^{18}O_{WATER\_\Delta47}$ is -1.8 ± 0.9‰ and -2.7 ± 1.2‰ in modern
240 and historical shells, respectively. Average measured river $\delta^{18}O$ was -2.1 ± 1.5‰ in 2012-2013.
241 Similar Δ_{47} values for historical and modern shells indicate growth intervals of similar average
242 water temperature.

243 **4. DISCUSSION**

244 ***4.1. Shell Growth Chronologies***

245 Preliminary shell growth chronologies have been constructed based on correlation
246 between measured and predicted shell $\delta^{18}O$ values, the latter being determined by river water
247 $\delta^{18}O$ and temperature measurements, and isotopic paleotemperature relations. Water $\delta^{18}O$
248 ($\delta^{18}O_{water}$) water temperature during the 2012-2013 period were measured by Van Plantinga et al.
249 (2016; Figure 4A). $\delta^{18}O_{water}$ ranges from -7.0 to 1.4‰, and temperature ranges from 6.7 to 37.8

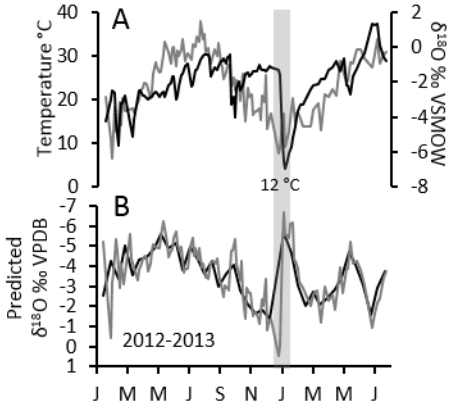

Figure 4. A. Water $\delta^{18}O$ and temperature from the Brazos River at Highway 60 near College Station for 2012-2013. B. Predicted $\delta^{18}O$ of aragonitic shell (gray line) with fortnightly averages (black line). The gray bar represents the timespan of 12 ˚C temperatures.

250 ˚C. Temperature and $\delta^{18}O_{water}$ covary significantly but not highly deterministically (r^2 = 0.28, N
251 = 120, $p < 0.05$). The covariance reflects (1) summer enrichment of ^{18}O due to increased
252 evaporation along with an increased proportion of evaporated, ^{18}O-enriched Lake Whitney water,
253 and (2) winter depletion of ^{18}O in response to a dominance of ^{18}O-depleted winter precipitation
254 and runoff (Chowdhury et al., 2010; Van Plantinga et al., 2016).

255 Predicted shell $\delta^{18}O$ values for 2012-2013 appear in Figures 4B, with values ranging
256 from -5.9 to 2.4‰, and fortnightly averages ranging from -5.4 to -1.4 ‰. The predicted
257 $\delta^{18}O_{SHELL}$ trend appears mostly temperature-driven in 2012, but values are more irregular in
258 2013, with low $\delta^{18}O_{SHELL}$ values due to a January rain storm and high values in June from
259 increased Lake Whitney flow. The $\delta^{18}O$ values for the shell transects fall in the same range as the
260 predicted values with generally a similar pattern. This suggests that shell is precipitated in
261 oxygen isotopic equilibrium with the water (as in Grossman and Ku, 1986; Dettman et al., 1999;
262 Goewert et al., 2007). As a first approximation, we have tied the three predicted $\delta^{18}O$ minima to
263 shell minima W, X, and Y, and tied the minimum at the shell edge (Z) to the minor predicted
264 $\delta^{18}O$ minimum in July 2013 (Figure 5). This age model (chronology 1) makes two implicit
265 assumptions. First, it assumes that extension rates associated with the milled transects are on the
266 order of 1 to 10 mm/year. Support for this assumption comes from studies by Christian et al.
267 (2000) and Haag and Rypel (2011), who found growth rates of 2-9 mm/yr for young adult
268 specimens of Threeridge mussels. Second, because winter extremes in the predicted $\delta^{18}O$ record
269 are not reproduced in the shell record, we introduce winter hiatuses within minima (peaks on
270 graph). For example, none of the mussel $\delta^{18}O$ records show the 0‰ value predicted in
271 December 2012 or the predicted -6‰ value predicted in early January 2013, thus we reconstruct
272 the *A. plicata* specimens (3R5 and 3R3) records with a hiatus in December 2012 growth.

Chronology 1 can be tested with the clumped isotope data. First we must consider the accuracy of the clumped isotope temperatures. Even if clumped isotope temperatures slightly overestimate ambient temperatures, relative temperatures should be reliable. In 3R5, Δ_{47} temperature trends agree well with trends in measured temperatures. Correlation points W, X, Y, and Z correlate with spring, winter, spring, and summer in Figure 5. Using this correlation, the

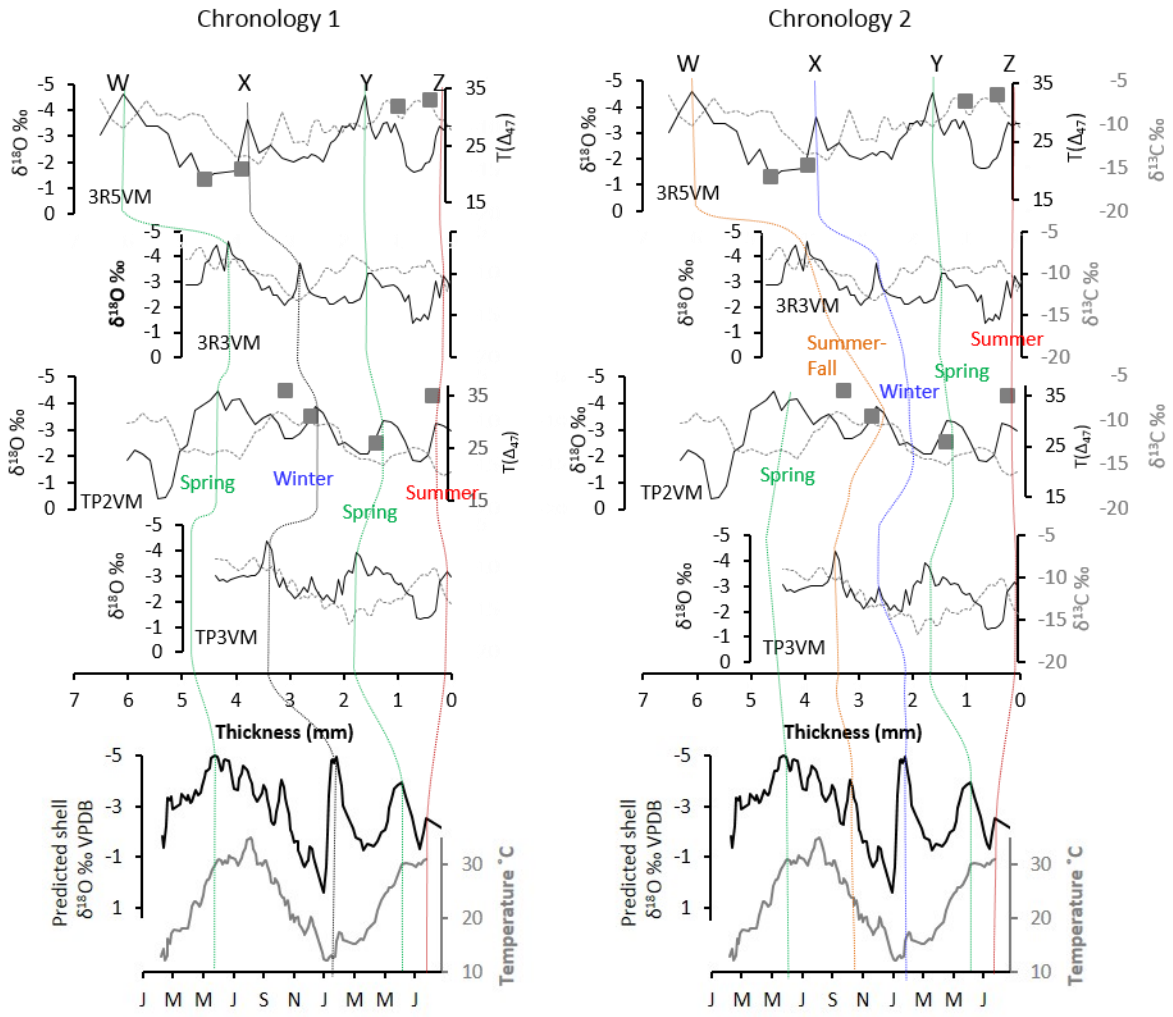

Figure 5. Oxygen (black line) and carbon (gray dashed line) isotope data, and clumped isotope temperature results (gray squares) in the four modern shells, along with fortnightly averages of measured temperatures and predicted shell $\delta^{18}O$ values. Tie points W, X, Y, Z connect hypothetical seasonal peaks and troughs in the data.

lowest clumped temperatures (19°, 21 °C) occur in fall or winter, and the warmest temperatures

(32°, 33 °C) occur in late spring and summer. For TP2VM, this age model only fits three of the five clumped temperature. The lowest Δ_{47} temperature for TP2VM is 26 °C. This is likely not from the part of the TP2VM record that grew under the coldest conditions, which were probably about the same as the coldest 3R5 clumped temperatures (20°C). Because 20°C (or 15 °C considering offset in T(Δ_{47})) does not reflect winter temperatures, our results suggest a winter slowing or cessation of growth rate corresponding to winter gaps in the shell growth chronologies. This does not rule out the possibility that strong winter rains and high discharge in January 2013, or low discharge (<500 cfs) and water level in November 2012, caused growth cessation, but it is consistent with the observance of winter growth cessation in other isotope studies (Dettman et al. 1999, Goewert et al., 2007). In Michigan and Netherlands mussels, cessation in shell growth was found to occur at ~12 °C and ~13.5 °C, respectively (Dettman et al., 1999, and Versteegh et al., 2010a). There is stable isotope evidence in the Brazos River shells for limited growth at daytime temperatures as low as 14 °C (February 2013), but not below 13.5 °C.

Chronology 1 makes a firm case for correlation between predicted and measured $\delta^{18}O$ records for 3R5VM and 3R3VM, but not for TP2VM and TP3VM records (Figure 5). For TP2VM, winter correlation (X) runs through a clumped isotope temperature that could fall on either side of the winter growth cessation (Fall 2012 or Spring 2013; Figure 6). An alternative age model for the TP2VM and TP3VM records (chronology 2) is shown in Figures 5 and 6, where the summer-winter 2012 interval (W-X) is expanded and the winter-spring 2013 interval (X-Y) is compressed. Chronologies 1 and 2 do not change the clumped isotope temperature chronology for TP2VM or the duration of the winter growth cessation in the *C. tampicoensis* shells, but chronology 2 shows timing of shell growth better supported by the clumped isotope evidence. For example, growth cessation in TP2VM occurs in late October according to chronology 2, rather than late September with chronology 1. With chronology 2, growth resumes in early March compared with early February using chronology 1. This is consistent

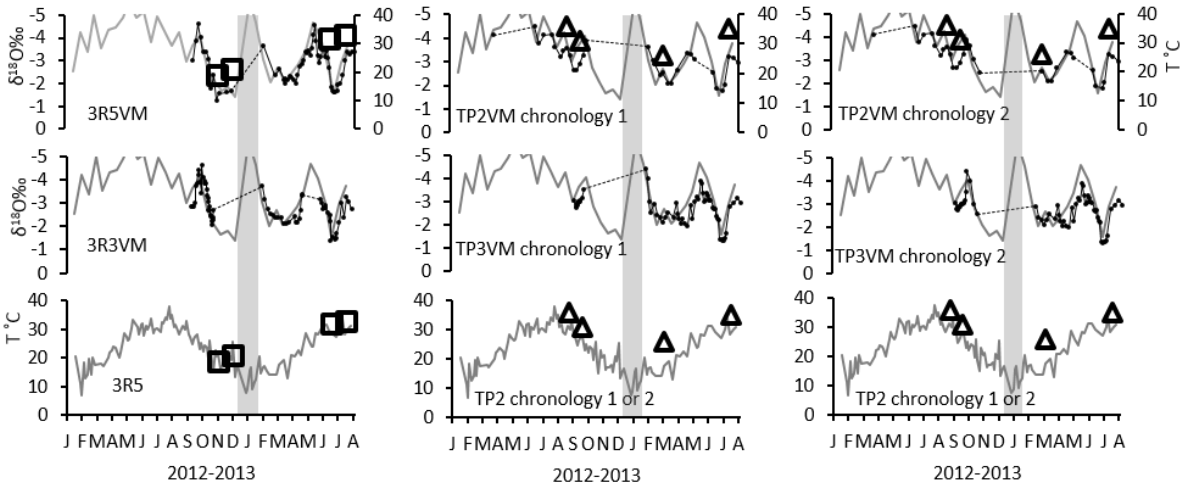

Figure 6. Comparison of the *A. plicata* sclerochronologies (3R5 and 3R3), and two possible *C. tampicoensis* sclerochronologies (TP2 and TP3). The gray bar represents the 12 ˚C temperature range. Note that the earlier portion of the TP2 record cannot be plotted on this time scale.

with the clumped isotope sample at 2.7 mm in TP2 and dated to September-October 2012 (31 ± 1 ˚C, or 26 ˚C if the calibration is adjusted). If this clumped isotope sample spanned the winter growth hiatus as implied in chronology 1, then it should have produced a significantly lower temperature.

The slightly shorter winter growth hiatuses in the Threeridge shells (54 and 98 days) than in the Tampico shells (124 and 116 days) is consistent with the geographic distribution of these species. Threeridge is found as far north as Minnesota and southern Canada (Hart et al., 2001; Mulcrone and Mehne, 2001) whereas the Tampico pearlymussel is native to Texas and northeastern Mexico (Howells, 2014). Thus, *A. plicata* may be more cold-tolerant than *C. tampicoensis*.

Eight of the nine $\delta^{18}O_{WATER\_\Delta47}$ estimates fall on the measured water $\delta^{18}O$ series (±0.6‰, ±14 days) when plotted according to the assigned shell growth chronologies (Figure 7). The discrepancy between observed and reconstructed $\delta^{18}O_{WATER\_\Delta47}$ values is worsened by adjusting the $T(\Delta_{47})$ values negatively to correct for the apparent positive offset in paleotemperature estimates. Despite the error associated with the clumped isotope temperatures (±4 °C), the trend

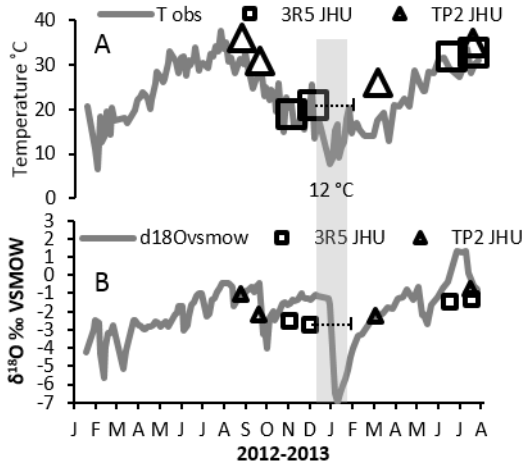

Figure 7. Clumped isotope temperature and water $\delta^{18}O$ chronologies (triangles, squares). Clumped isotope temperatures (A) and $\delta^{18}O_{WATER\_\Delta47}$ (B) chronologies combining 3R5 and TP2 data, based on the shell $\delta^{18}O$ chronologies. The gray bar represents the time period with 12 ˚C temperatures, and the 3R5 sample that overlaps with that time actually spans the winter growth hiatus.

in observed water data is roughly reproduced by the $\delta^{18}O_{WATER\_\Delta47}$ sclerochronology, though at lower resolution.

4.2. Shell Growth Rate

We attempted to age the shells by counting their light and dark growth bands as described in Neves and Moyer (1988), but ambiguity in the modern shell banding in these specimens makes this method dubious here. Nevertheless, the stable isotope data consistently suggested winter growth hiatuses in these species, highlighting variable shell growth rate and gaps in shell records from growth cessation. In the absence of time-consuming mark-recapture studies that produce empirical shell growth rates (Goewert et al., 2007; Haag and Commens-Carson, 2008; Haag, 2009), clumped isotope temperatures combined with micromilled oxygen isotope chronologies can provide detailed information on shell growth patterns in situations where neither shell growth bands nor cycles in shell $\delta^{18}O$ are reliable time markers.

The four modern shell ages are 3-4 years based on the stable isotope chronologies. These ages are 1-4 years younger than those obtained by counting growth bands and using the growth constants from Haag and Rypel (2011). Admittedly, identifying distinct annual growth bands in these modern specimens was too difficult to estimate age with confidence. Growth rate results here support findings of other stable isotope studies and mark-recapture studies in which counting bivalve growth bands overestimated shell age and underestimated shell growth rate because of the tendency to misidentify stress bands - or false annuli deposited when mussels are suddenly disturbed - as real annuli (Downing et al., 1992; Goewert and Surge, 2008; Haag and Commens-Carson, 2008).

341 The shell growth models in Table 1 suggest either of two possibilities: (1) the modern
342 shells have higher Bertalanffy growth constants (*K* values for growth rate) than the historical
343 shells, or (2) the asymptotic size limits (L_{inf}) of the modern shells is greater than the historical
344 shells. We base Tampico L_{inf} on Howells (2014) and Threeridge L_{inf} on Haag and Rypel (2011).
345 The comparisons here are limited by inadequate sample sizes, and the historical shells cannot be
346 aged by the same standards of isotopic microsampling precision as the modern shells. However,
347 the annual growth bands stand out more distinctly in the older historical shells (Figure 2),
348 making the band-counting method more viable for bracketing the shell age. To test how realistic
349 our *K* estimates are and to account for the tendency of band-counting to overestimate shell age,
350 we give ranges of historical shell ages where the lower limit of possible shell age is one year
351 younger than the banding indicates. Phenotypes within the same species in the same ecosystem
352 are known to vary widely by growth rate (Haag and Rypel, 2011). Relocation studies show that
353 environmental change influences mussel shell growth rate (Kesler et al., 2007).

354 Chronology 1 yields average growth rates (measured as thickening rates as in Dettman et
355 al. (1999)) of 0.7 mm/month for 3R5VM, 0.9 mm/month for 3R3VM, 0.5 mm/month for
356 TP2VM, and 0.9 mm/month for TP3VM. These estimates include averaging 0 mm/month
357 growth rates for months with no growth. Chronology 2 estimates average growth rates of 0.5
358 mm/month for TP2VM and 0.7 mm/month for TP3VM. Monthly growth rates in mm of shell
359 thickness are plotted in Figure 8. These values are susceptible to as much as 50% error
360 depending on: 1) sampling resolution, 2) how the micromilled $\delta^{18}O$ values are aligned with
361 predicted values, and 3) how growth rates are consequently binned in different months. The
362 estimated growth rates are highest in the late spring and mid-fall, which are historically the times
363 of greatest rainfall although not during the study period. No relationship was observed between

our shell growth rates and river discharge rates and water temperature. Although shear stress has been related to mussel growth rate in the past (Layzer and Madison, 1995; Strayer, 1999), the water velocity at specific mussel sites (e.g., backwater or bank margin habitats) may vary independently of more spatially generalized river variables like discharge. Higher turbidity tied to high discharge could slow or stop feeding and shell growth (Kaandorp et al., 2003; Kelemen et al., 2017). Alternative growth rate factors include feeding, reproduction, and ontogeny (Dettman et al., 1999). Links between shell growth rate and primary productivity should be explored in future studies.

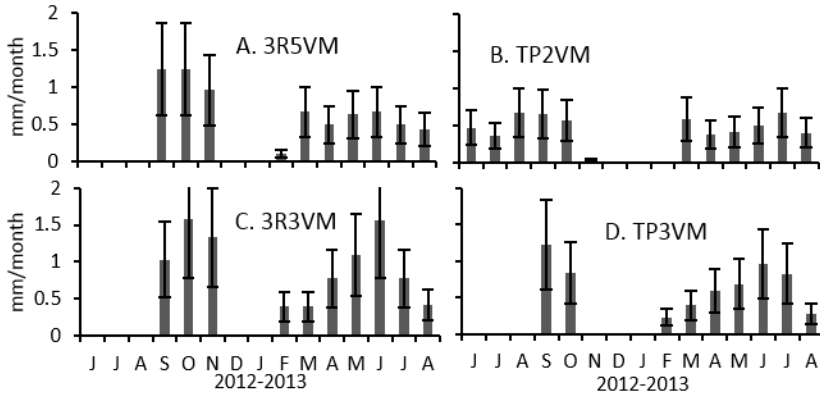

Figure 8. Monthly average shell growth rates in mm/month of cumulative shell thickness (as sampled by the micromill) in the shell z-plane perpendicular to the axes of shell length and width, with 50% error bars. Growth rates are based on the stable isotope chronologies (chronology 1 for 3R5 and 3R3 (*A. plicata*) and chronology 2 for TP2 and TP3 (*C. tampicoensis*)).

4.3. Carbon Isotopes

The mean $\delta^{13}C$ values of ventral margins of *A. plicata* (~ -9‰) and *C. tampicoensis* (~ -12‰) depend on the $\delta^{13}C$ of river DIC ($\delta^{13}C_{DIC}$) and the proportion of metabolically-derived carbon (roughly -25‰) in the shell (McConnaughey and Gillikin, 2008). Brazos River $\delta^{13}C_{DIC}$ values in Brazos County in 1989 (B.K. Kaufman and E.L. Grossman, unpublished data) and between 2007 and 2009 (Zeng et al., 2010) are all between -6 and -9‰. With an aragonite-bicarbonate ^{13}C fractionation factor of about 2.7‰ (Romanek et al., 1992), this predicts shell equilibrium $\delta^{13}C$ values of about -3 to -6‰, much higher than the observed shell values except for the Threeridge umbo area (~-6‰). Higher $\delta^{13}C$ values in juvenile portions of mollusks are

common (e.g., Gillikin et al., 2007; Gentry et al., 2008) and suggest less metabolic carbon incorporation into the shell prior to sexual maturity. The proportion of metabolic carbon (C_M) incorporated in the shell can be calculated using a mass balance equation and assuming a baseline $\delta^{13}C_{DIC}$ of -7.5‰, metabolic carbon ($\delta^{13}C_M$) of -25‰, and a 2.7‰ enrichment of aragonite relative to bicarbonate (ε):

$$C_M = (\delta^{13}C_{shell} - \varepsilon - \delta^{13}C_{DIC}) / (\delta^{13}C_M - \delta^{13}C_{DIC}) \quad (5)$$

This calculation indicates ~20% incorporation of metabolic carbon in *A. plicata* shells and ~40% in *C. tampicoensis* shells. These percent metabolic carbon estimates fall into the range that McConnaughey and Gillikin (2008) characterize as higher percentages (>10%) and what Dettman et al. (1999) suggest is a consequence of mussel maturity and reproductive behavior, like seasonal brooding. No correlation was observed between shell $\delta^{13}C$ and $\delta^{18}O$ to suggest kinetic effect as was observed in Goewert et al. (2007).

Based on the $\delta^{18}O$ correlations (Figure 3), the $\delta^{13}C$ curves are similar within species but not between species. This suggests that shells of the same species are responding to the same environmental ($\delta^{13}C_{DIC}$) and/or physiological (e.g., spawning) factors, and could be used as a chronometer if the timing of the $\delta^{13}C$ influences for individual taxa are known. Lake Whitney water represents an upper end-member value of $\delta^{13}C_{DIC}$ (~ -6‰, Zeng et al., 2011) compared with Brazos River values measured in the study area previously. Though we lack time series data for $\delta^{13}C_{DIC}$ during our study interval, the dominance of Lake Whitney discharge during low flow conditions in summer (Van Plantinga et al., 2016) should produce a seasonal $\delta^{13}C_{DIC}$ maxima, in contrast to other seasons when Brazos River discharge is dominated by runoff with low $\delta^{13}C_{DIC}$. The sclerochronology assigned for *A. plicata* shows $\delta^{13}C$ is high in the summer and low in the

winter, the relationship predicted by Lake Whitney discharge patterns. Thus, carbon isotopes in Brazos River mussels may be useful in developing chronologies; however, the potential for vital effects on $\delta^{13}C$ makes it a less effective proxy than $\delta^{18}O$ and Δ_{47}.

4.4. Environmental Reconstruction and Dam Impacts

Using mussel isotope values and actual records of river flow, we reconstructed Brazos River high-discharge events patterns and water source as percentage of Lake Whitney water (%LW) in Brazos River discharge (*Q*) in College Station. The %LW is also a salinity proxy because Lake Whitney is a high salinity endmember (Chowdhury et al., 2010; Van Plantinga et al., 2016). Excluding specimen TP2, for which fewer analyses are available, $\delta^{13}C$ correlates positively with %LW and $\delta^{18}O$ correlates negatively with discharge. Major trends in %LW can be reconstructed using a $\delta^{13}C$-%LW linear regression equation – derived from 3R5VM, 3R3VM, and TP3 – and a composite $\delta^{13}C$ record from those three shells (Table 4; Figure 9B). Despite that

Table 4. Pearson's R values (bold black are significant, $p < 0.02$) for linear relationships between isotope values and river parameters, slopes (m) and intercepts (b) for discharge (Q), percent of flow from Lake Whitney (%LW), and electrical conductivity (EC) in µS/cm.

		Q			%LW			EC			
Sample		R	m	b	R	m	b	R	m	b	N
3R5	$\delta^{13}C$	0.08			**0.36**	0.08	0.99	0.20			58
	$\delta^{18}O$	**-0.49**	-253	-132	0.15			**0.46**	144	1246	58
3R3	$\delta^{13}C$	**0.39**	118	1706	**0.40**	0.11	1.31	**0.40**	58	1422	68
	$\delta^{18}O$	**-0.32**	-188	25	0.20			0.12			68
TP2	$\delta^{13}C$	0.07			0.10			0.40			32
	$\delta^{18}O$	-0.34			-0.03			0.05			32
TP3	$\delta^{13}C$	**0.34**	77	1687	**0.48**	0.08	1.36	**0.77**	101	2087	61
	$\delta^{18}O$	**-0.47**	-363	-258	**0.42**	0.24	1.00	0.19			61

Tampico shells probably have more metabolic carbon than Threeridgee shells, Table 4 shows similar %LW-$\delta^{13}C$ relationships across shell species. Figure 9A shows that there is a significant

417 temperature-$\delta^{13}C$ relationship in *A. plicata* shells which is not seen in *C. tampicoensis*. The
418 reconstruction is inaccurate, but the sustained periods of low and high %LW are successfully
419 identified. It is a more accurate reconstruction than if only the Threeridge specimens are used but
420 not TP3. This suggests that there are differences in seasonal (temperature-related) metabolic
421 activity between the two species studied here, but that shell $\delta^{13}C$ values in both species are
422 similarly influenced by river $\delta^{13}C_{DIC}$ which is in turn driven by %LW.

423 We reconstructed Brazos River flow patterns in the manner of Versteegh et al. (2010b)
424 by using the Brazos River discharge-water $\delta^{18}O$ relationship. Figure 9C shows that this
425 relationship is heteroscedastic below about -2.4‰, posing problems for regression models.
426 However, the yearly and October-April data sets still show significant relationships ($p < 0.05$).
427 Shell $\delta^{18}O$ and Δ_{47} chronologies were converted into water $\delta^{18}O$ chronologies assuming
428 sinusoidal seasonal temperature variation. The reconstructed water $\delta^{18}O$ can in turn reconstruct
429 discharge using the observed relationship for October-April:

430 $$\delta^{18}O = -0.566\ln(Q) + 0.99 \quad (6)$$

where *Q* is river discharge in cubic feet per second (cfs). This was done by combining the $\delta^{18}O$

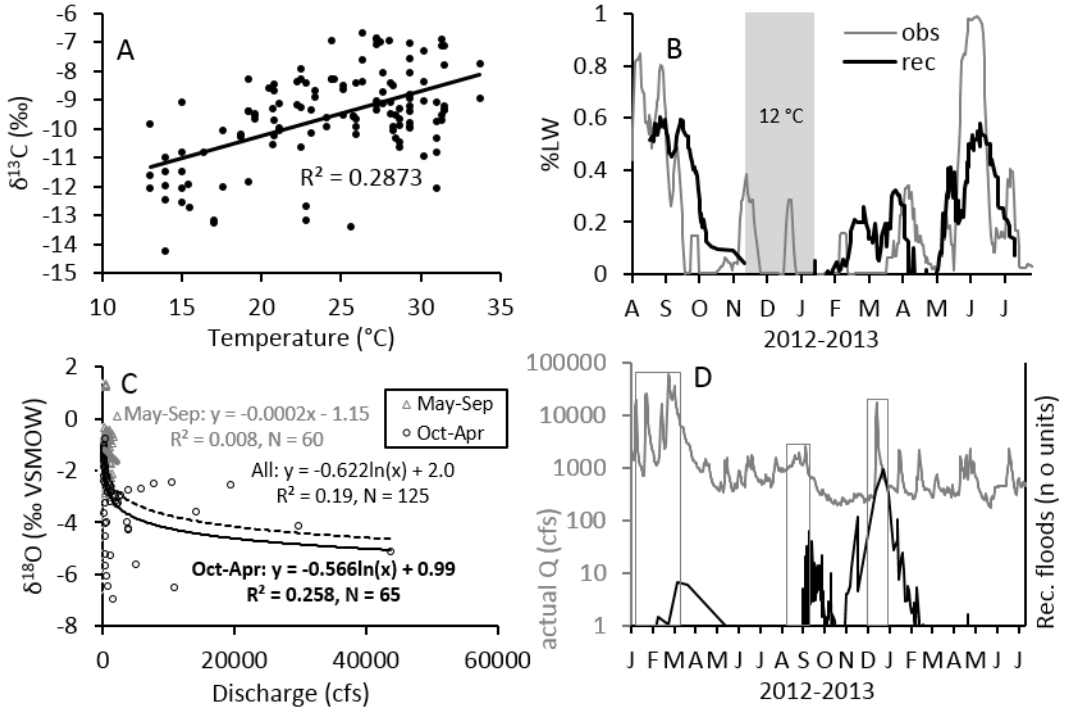

Figure 9. (A) Modern Threeridge, 3R5 and 3R3 combined, water temperature vs. shell $\delta^{13}C$ (regression $p < 0.05$). (B) Reconstructed (black) and actual (gray) weekly averages of percent Lake Whitney water (%LW) based on composite of 3R5, 3R3, and TP3 $\delta^{13}C$ chronologies. Gray fill covers the winter growth cessation. (C) Brazos River discharge vs. $\delta^{18}O$. Logarithmic correlation between discharge in cubic feet per second (cfs) and water $\delta^{18}O$ for 2012-2013 in the Brazos River near Bryan-College Station. (D) Actual discharge in 2012-2013 in gray and discharge reconstructed from shell $d^{18}O$ values and seasonal temperature using the method from Versteegh et al. (2010) in black. Two categories of high discharge are shown in the gray rectangles: very high discharge (>10000 cfs), and sustained high discharge (>1000 cfs for >10 days), although the reconstructed high-discharge events do not distinguish between the two categories.

chronologies from the ventral margins of all four modern shells into a single "master" isotope chronology. This master chronology was combined with sinusoidal seasonal temperature (Equation 7) estimates using Equations 2-4. Temperature was reconstructed by date as follows:

$$T\ (°C) = 9 * \cos(\text{date}/56.88) + 23 \quad (7)$$

where date is days after 1900 as in Microsoft Excel (version 2010). In relating $\delta^{18}O$ to discharge we chose to use the relationship for the October-April data rather than the warm or cool relationships because there is no significant relationship in May-September so only high-discharge events in October-April can be identified (Figure 9D). The Brazos is subject to strong influence from reservoir flow in summer and storm runoff in winter, in contrast to the wintertime dominance of groundwater in the River Meuse in the Netherlands (Versteegh et al., 2010b). While Versteegh et al. (2010b) and Kelemen et al. (2017) reconstructed low summer discharge, we use this method to identify high-discharge events in fall, winter, and spring.

In Figure 9D, the maximum flow events in March 2012 and January 2013 are successfully identified using the method from Versteegh et al. (2010b). Two types of high-discharge events are identified: 1) sustained high-flow events, where discharge stays above 1,000 cfs for 10 days or more; and 2) very high flow events, where discharge exceeds 10,000 cfs. Average discharge for the study period was 1,943 cfs. Our treatment of shell data does not accurately quantify Brazos River discharge (hence no units in right scale of Figure 9D), but the approach does identify high-discharge events. Identifying freshwater discharge maxima can make shell-growth chemistry records valuable tools for reconstructing ancient river flow and water salinity patterns (Dettman et al., 2004). However, there are clearly significant sources of error associated with shell age assignments, temperature assignments, and seasonal and ontogenetic biases in how consistently the shells record environmental conditions.

Sclerochronological reconstructions of river discharge by Versteegh et al. (2010b) and Kelemen et al. (2017) focused on accurately reconstructing flow measurements during seasonally low discharge while high discharge was not reconstructed as accurately. These studies took place in environments well-suited for sclerochronology because seasonal water $\delta^{18}O$ and temperature

patterns combined to produce distinct cycles in shell $\delta^{18}O$. By contrast, water $\delta^{18}O$ and temperature patterns in the Brazos River in 2012-2013 produce an irregular, non-periodic $\delta^{18}O$ signal, the result of subtropical climate, intense regulation, and the lack of significant catchment of low-$\delta^{18}O$ precipitation in its upper watershed (*sensu* Dutton et al., 2005). Consequently, Brazos River mussel shells have unreliable annual growth banding and exhibit a weak relationship between river discharge and shell $\delta^{18}O$ compared with other rivers (Versteegh et al., 2010b; Kelemen et al., 2017).

Our study period coincided with the Texas drought that began in 2011 and persisted through 2014. Low runoff or high dam release rates affected river flow components, and evaporation elevated water $\delta^{18}O$ (Chowdhury et al., 2010; Van Plantinga et al., 2016). The significant differences between modern and historical shell $\delta^{18}O$ and $\delta^{18}O_{WATER\_\Delta47}$ support the hypothesis that drought and impoundment in 2012-2013 increased these values. It is difficult to determine if $\delta^{18}O$ differences between modern and historic shells reflect the impact of impoundment of waters, modern drought, or a combination of the two without better understanding of the climate conditions at the time of collection of historic shells.

Relationships between various isotopic measurements ($\delta^{13}C$, $\delta^{18}O$, Δ_{47}) for modern and historical shells provide an opportunity to contrast river hydrology before and after dam construction in the watershed. Overall, $\delta^{18}O$ is correlated with Δ_{47} reflecting the inverse relationship between $\delta^{18}O$ and temperature (Figure 10A). Remaining variance in $\delta^{18}O$ and Δ_{47} within and between samples reflects variability in water $\delta^{18}O$ and error in Δ_{47}. For the overlapping temperature range (23-38 °C), modern shells average ~0.9 ‰ higher in $\delta^{18}O$ (Table 3), reflecting greater evaporation due to dammed lakes and/or drought. There is no difference in average $\delta^{13}C$ between modern and historical shells, suggesting similar $\delta^{13}C_{DIC}$. This could

represent similarities in carbon cycling or perhaps offsetting modern influences of increased anthropogenic CO_2 and increased atmospheric exchange with impoundment. Interestingly, historical shells show a linear relation between $\delta^{13}C$ and Δ_{47} not seen in the modern shells (Figure 10B). This suggests that prior to dam construction, $\delta^{13}C_{DIC}$ was lower in summer and higher in winter, opposite the trend observed in the river today (Figure 5; Figure 9A) due to the greater contribution of ^{13}C-enriched Lake Whitney water in summer (Zeng et al., 2011).

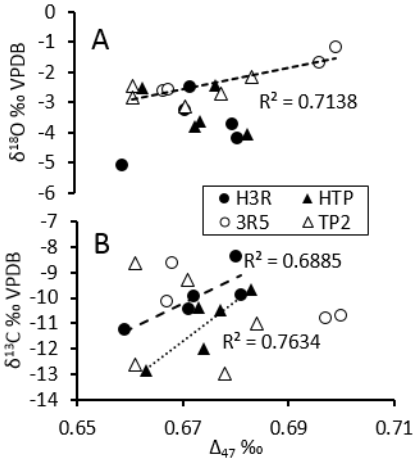

Figure 10. Oxygen (A) and carbon (B) isotopic compositions versus Δ_{47} for modern and historic shells. The dashed line in A is for modern shells only. The dashed line in B is for H3R and the dotted line is for HTP. Level of significance (p) for regressions <0.05.

Our historical-modern comparisons are limited by the short time interval represented by the isotopic record. Furthermore, because we compare ~10 year old growth in historical shells with 3-4 year old growth in modern shells, carbon isotope differences may be influenced by ontogenetically-controlled vital effects. Nevertheless, the isotopic differences between our historical and modern shells highlight the potential of this approach to explore the hydrology of ancient river systems.

5. CONCLUSIONS

The $\delta^{18}O$ profiles of four modern freshwater mussel shells show similar values and trends with shell growth. Furthermore, intra-shell comparisons between the inner nacreous and outer nacreous regions yield nearly identical $\delta^{18}O$ records regardless of species. This validates shell

$\delta^{18}O$ as an environmental archive and chronometer. We also observed consistent intra-shell and inter-shell $\delta^{13}C$ trends, but differences between species. Carbon isotope values are consistently lower in *Cyrtonaias tampicoensis* compared with *Amblema plicata*, suggesting greater incorporation of metabolic carbon in shells of the former. Despite the incorporation of metabolic carbon in shells (up to 40%), we see evidence that seasonal patterns in upstream dam releases influence the $\delta^{13}C$ of DIC and consequently shell $\delta^{13}C$.

Clumped isotope temperatures of shell growth layers can be used to determine the seasons in which shell segments grew. The use of clumped isotopes improves the accuracy of sclerochronology, especially where shell $\delta^{18}O$ records are complex due to impoundment of water, variable runoff, and winter growth slowing or cessation. Proposed heuristic growth chronologies are consistent with expected seasonal growth patterns (i.e., winter growth hiatuses). Based on isotopic sclerochronologies, shell thickening rates in young adult individuals are approximately 0.5 mm/month on average and reach as high as 2 mm/month during the spring-fall period.

We were able to reconstruct the timing of high river discharge with $\delta^{18}O$ and water source variability with $\delta^{13}C$, demonstrating the utility of mussel shell $\delta^{18}O$ and $\delta^{13}C$ for paleohydrologic reconstruction. Shell $\delta^{18}O$ and $\delta^{18}O_{WATER\_}\Delta47$ were lower in historical shells collected before intensive damming than in the modern shells. This reflects enhanced evaporation likely due to modern impoundment of river water as well as the impact of the drought of 2011-12.

ACKNOWLEDGEMENTS

519 The authors would like to thank the Michel T. Halbouty Chair in Geology at Texas A&M
520 University for supporting this research. Charles Randklev and Eric Tsakiris collected the mussel
521 specimens. Ann Molineux from UTA NPL provided historical specimens from the Singley-
522 Askew Collection. Charles Randklev and Robert G. Howells provided helpful perspective on
523 mussel ecology. Ben Passey, Naomi Levin, Huanting Hu, Haoyuan Ji, Sophie Lehmann, Dana
524 Brenner, and Lai Ming provided valuable assistance at the Johns Hopkins University Stable
525 Isotope Lab. Chris Maupin, Lauren Graniero, Andrew Roark, and Brendan Roark helped run
526 isotope samples at the Stable Isotope Geoscience Facility at Texas A&M University. Clumped
527 isotope analyses were financed by NSF grant EAR-1226918. Data reported here are in the
528 following online repository: earthchem.org. We thank the reviewers for their helpful advice.

529 **REFERENCES**

530 Carroll, M., C. Romanek, and L. Paddock (2006), The relationship between the hydrogen and
531 oxygen isotopes of freshwater bivalve shells and their home streams, *Chemical Geology*,
532 *234*(3-4), 211-222, doi:10.1016/j.chemgeo.2006.04.012.

533 Chowdhury, A., Osting, T., Furnans, J., Mathews, R. (2010), Groundwater-surface water
534 interaction in the Brazos River Basin: Evidence from lake connection history and
535 chemical and isotopic compositions, *Texas Water Development Board Report*,
536 *375*(August), 61.

537 Christian, A. D., C. L. Davidson, I. Posey, R. William, P. J. Rust, J. L. Farris, J. L. Harris, and L.
538 Harp (2000), Growth curves of four species of commercially valuable freshwater mussels
539 (Bivalva: Unionidae), *Journal of the Arkansas Academy of Science*, *54*(1), 41-50.

Dennis, K. J., H. P. Affek, B. H. Passey, D. P. Schrag, and J. M. Eiler (2011), Defining an absolute reference frame for 'clumped' isotope studies of CO_2, *Geochimica et Cosmochimica Acta*, *75*(22), 7117-7131.

Dettman, D. L., and K. C. Lohmann (1995), Microsampling carbonates for stable isotope and minor element analysis: Physical separation of samples on a 20 micrometer scale: *Journal of Sedimentary Research*, *65*(3).

Dettman, D. L., A. K. Reische, and K. C. Lohmann (1999), Controls on the stable isotope composition of seasonal growth bands in aragonitic fresh-water bivalves (Unionidae), *Geochimica et Cosmochimica Acta*, *63*(7), 1049-1057.

Dettman, D. L., K. W. Flessa, P. D. Roopnarine, B. R. Schöne, and D. H. Goodwin (2004), The use of oxygen isotope variation in shells of estuarine mollusks as a quantitative record of seasonal and annual Colorado River discharge, *Geochimica et Cosmochimica Acta*, *68*(6), 1253-1263.

Downing, W. L., J. Shostell, and J. A. Downing (1992), Non-annual external annuli in the freshwater mussels *Anodonta grandis grandis* and *Lampsilis radiata siliquoidea*, *Freshwater Biology*, *28*(3), 309-317.

Dutton, A., B. H. Wilkinson, J. M. Welker, G. J. Bowen, and K. C. Lohmann (2005), Spatial distribution and seasonal variation in18O/16O of modern precipitation and river water across the conterminous USA, *Hydrological Processes*, *19*(20), 4121-4146.

Epstein, S., Buchsbaum, R., Lowenstam, H., H. Urey (1953), Revised carbonate-water isotopic temperature scale. *GSA Bulletin, 64 (11)*, 1315-1326.

561 Freeman, M. C., C. M. Pringle, E. A. Greathouse, and B. J. Freeman (2003), Ecosystem-level
562 consequences of migratory faunal depletion caused by dams, paper presented at
563 American Fisheries Society Symposium.
564 Gentry, D. K., S. Sosdian, E. L. Grossman, Y. Rosenthal, D. Hicks, and C. H. Lear (2008),
565 Stable isotope and Sr/Ca profiles from the marine gastropod *Conus ermineus*: Testing a
566 multiproxy approach for inferring paleotemperature and paleosalinity, *Palaios*, *23*(3-4),
567 195-209.
568 Gillikin, D. P., A. Lorrain, L. Meng, and F. Dehairs (2007), A large metabolic carbon
569 contribution to the $\delta^{13}C$ record in marine aragonitic bivalve shells, *Geochimica et*
570 *Cosmochimica Acta*, *71*(12), 2936-2946.
571 Goewert, A., D. Surge, S. J. Carpenter, and J. Downing (2007), Oxygen and carbon isotope
572 ratios of *Lampsilis cardium* (Unionidae) from two streams in agricultural watersheds of
573 Iowa, USA, *Palaeogeography, Palaeoclimatology*, *Palaeoecology*, *252*(3), 637-648.
574 Goewert, A. E., and D. Surge (2008), Seasonality and growth patterns using isotope
575 sclerochronology in shells of the Pliocene scallop *Chesapecten madisonius*, *Geo-Marine*
576 *Letters*, *28*(5-6), 327-338.
577 Gonfiantini, R., Stichler, W., K. Rozanski (1995), Standards and intercomparison materials
578 distributed by the International Atomic Energy Agency for stable isotope
579 measurements (IAEA-TECDOC--825). International Atomic Energy Agency (IAEA).
580 Grossman, E. L., and T.-L. Ku (1986), Oxygen and carbon isotope fractionation in biogenic
581 aragonite: temperature effects, *Chemical Geology: Isotope Geoscience section*, *59*, 59-74.

582 Haag, W. R., and A. M. Commens-Carson (2008), Testing the assumption of annual shell ring
583 deposition in freshwater mussels, *Canadian Journal of Fisheries and Aquatic Sciences*,
584 *65*(3), 493-508.
585 Haag, W. R. (2009), Extreme longevity in freshwater mussels revisited: sources of bias in age
586 estimates derived from mark-recapture experiments, *Freshwater Biology*, *54*(7), 1474-
587 1486, doi:10.1111/j.1365-2427.2009.02197.x.
588 Haag, W. R., and A. L. Rypel (2011), Growth and longevity in freshwater mussels: evolutionary
589 and conservation implications, *Biological reviews of the Cambridge Philosophical*
590 *Society*, *86*(1), 225-247, doi:10.1111/j.1469-185X.2010.00146.x.
591 Haag, W. R. (2012), *North American freshwater mussels: natural history, ecology, and*
592 *conservation*, Cambridge University Press.
593 Hart, R.A., Grier, J.W., Miller, A.C., Davis, M., 2001. Empirically derived survival rates of a
594 native mussel, *Amblema plicata*, in the Mississippi and Otter Tail Rivers, Minnesota. *The*
595 *American Midland Naturalist, 146*, 254-263.
596 Henkes, G. A., B. H. Passey, A. D. Wanamaker, E. L. Grossman, W. G. Ambrose, and M. L.
597 Carroll (2013), Carbonate clumped isotope compositions of modern marine mollusk and
598 brachiopod shells, *Geochimica et Cosmochimica Acta*, *106*, 307-325,
599 doi:10.1016/j.gca.2012.12.020.
600 Howells, R. G (2014), *Field Guide to Texas Freshwater Mussels*, BioStudies, Kerville, Texas.
601 Ivany, L. C., B. H. Wilkinson, K. C. Lohmann, E. R. Johnson, B. J. McElroy, and G. J. Cohen
602 (2004), Intra-annual isotopic variation in Venericardia bivalves: Implications for early
603 Eocene temperature, seasonality, and salinity on the US Gulf Coast, *Journal of*
604 *Sedimentary Research*, *74*(1), 7-19.

605 Kaandorp, R. J., H. B. Vonhof, C. Del Busto, F. P. Wesselingh, G. M. Ganssen, A. E. Marmól,
606 L. R. Pittman, and J. E. van Hinte (2003), Seasonal stable isotope variations of the
607 modern Amazonian freshwater bivalve *Anodontites trapesialis*, *Palaeogeography,*
608 *Palaeoclimatology, Palaeoecology*, *194*(4), 339-354.
609 Keating-Bitonti, C. R., L. C. Ivany, H. P. Affek, P. Douglas, and S. D. Samson (2011), Warm,
610 not super-hot, temperatures in the early Eocene subtropics, *Geology*, *39*(8), 771-774,
611 doi:10.1130/g32054.1.
612 Kelemen, Z., D. P. Gillikin, L. E. Graniero, H. Havel, F. Darchambeau, A. V. Borges, A.
613 Yambélé, A. Bassirou, and S. Bouillon (2017), Calibration of hydroclimate proxies in
614 freshwater bivalve shells from Central and West Africa, *Geochimica et Cosmochimica*
615 *Acta*, *208*, 41-62.
616 Kesler, D. H., T. J. Newton, and L. Green (2007), Long-term monitoring of growth in the
617 Eastern Elliptio, *Elliptio complanata* (Bivalvia: Unionidae), in Rhode Island: a transplant
618 experiment, *Journal of the North American Benthological Society*, *26*(1), 123-133.
619 Layzer, J. B., and L. M. Madison (1995), Microhabitat use by freshwater mussels and
620 recommendations for determining their instream flow needs, *Regulated Rivers: Research*
621 *& Management*, *10*(2-4), 329-345.
622 Lydeard, C., R. H. Cowie, W. F. Ponder, A. E. Bogan, P. Bouchet, S. A. Clark, K. S. Cummings,
623 T. J. Frest, O. Gargominy, and D. G. Herbert (2004), The global decline of nonmarine
624 mollusks, *BioScience*, *54*(4), 321-330.
625 McConnaughey, T. A., and D. P. Gillikin (2008), Carbon isotopes in mollusk shell carbonates,
626 *Geo-Marine Letters*, *28*(5-6), 287-299, doi:10.1007/s00367-008-0116-4.

Mulcrone, R. S., and C. Mehne (2001), Freshwater mussels of the Kalamazoo River, Michigan, from Battle Creek to Saugatuck. Prepared for U.S. Fish and Wildlife Service.

Neves, R. J., and S. N. Moyer (1988), Evaluation of techniques for age determination of freshwater mussels (Unionidae), *American Malacological Bulletin*, *6*(2), 179-188.

Nielsen-Gammon, J. W. (2011), The changing climate of Texas, in *The impact of global warming on Texas. University of Texas Press, Austin*, edited, pp. 39-68.

Randklev, C. R., M. S. Johnson, E. T. Tsakiris, J. Groce, and N. Wilkins (2013), Status of the freshwater mussel (Unionidae) communities of the mainstem of the Leon River, Texas, *Aquatic Conservation: Marine and Freshwater Ecosystems*, *23*(3), 390-404, doi:10.1002/aqc.2340.

Richter, B. D., D. P. Braun, M. A. Mendelson, and L. L. Master (1997), Threats to imperiled freshwater fauna, *Conservation Biology*, *11*(5), 1081-1093.

Romanek, C. S., E. L. Grossman, and J. W. Morse (1992), Carbon isotopic fractionation in synthetic aragonite and calcite: effects of temperature and precipitation rate, *Geochimica et Cosmochimica Acta*, *56*(1), 419-430.

Schöne, B. R. (2003), A 'clam-ring'master-chronology constructed from a short-lived bivalve mollusc from the northern Gulf of California, USA, *The Holocene*, *13*(1), 39-49.

Strayer, D. L. (1999), Use of flow refuges by unionid mussels in rivers, *Journal of the North American Benthological Society*, *18*(4), 468-476.

Tsakiris, E. T., and C. R. Randklev (2016), Structural changes in freshwater mussel (Bivalvia: Unionidae) assemblages downstream of Lake Somerville, Texas, *The American Midland Naturalist*, *175*(1), 120-127.

649 VanPlantinga, A., E.L. Grossman, and E. B. Roark (2016), Chemical and isotopic tracer
650 evaluation of water mixing and evaporation in a dammed Texas River during drought.
651 *River Research and Applications*.
652 Vaughn, C. C., and C. M. Taylor (1999), Impoundments and the decline of freshwater mussels: a
653 case study of an extinction gradient, *Conservation Biology*, *13*(4), 912-920.
654 Versteegh, E. A., H. B. Vonhof, S. R. Troelstra, R. J. Kaandorp, and D. Kroon (2010),
655 Seasonally resolved growth of freshwater bivalves determined by oxygen and carbon
656 isotope shell chemistry, *Geochemistry, Geophysics, Geosystems*, *11*, 8022.
657 Versteegh, E. A. A., H. B. Vonhof, S. R. Troelstra, and D. Kroon (2010), Can shells of
658 freshwater mussels (Unionidae) be used to estimate low summer discharge of rivers and
659 associated droughts?, *International Journal of Earth Sciences*, *100*(6), 1423-1432,
660 doi:10.1007/s00531-010-0551-0.
661 Ward, G. H. (2012), Water Resources and Water Supply, in *The Impact of Global Warming on*
662 *Texas*, edited by J. N. Schmandt, Gerald R.; Clarkson, Judith, pp. 69-95, University of
663 Texas Press, Austin.
664 Zeng, F.-W., C. A. Masiello, and W. C. Hockaday (2011), Controls on the origin and cycling of
665 riverine dissolved inorganic carbon in the Brazos River, Texas, *Biogeochemistry*, *104*(1-
666 3), 275-291.